Characterization and magnetic properties of $Fe_{1-x}Ni_x$ nanowire arrays

Qingfang Liu,* Jianbo Wang, Zhongjie Yan, and Desheng Xue

Key Laboratory for Magnetism and Magnetic Materials of MOE, Lanzhou University, Lanzhou 730000, People's Republic of China

Detailed fabrication, structure, and magnetic properties of $Fe_{1-x}Ni_x$ nanowire arrays were investigated. The dependence of structural variation on the Ni content was determined by x-ray diffraction, showing different behaviors of nanowire arrays from the bulk and particle systems. The magnetic properties in the temperature range of 5 to 300 K were studied and results show the coercivity at 300 K does not monotonically decrease as Ni content increases. When the applied field is along the long axis, the temperature dependence of coercivity for $Fe_{0.68}Ni_{0.32}$ and $Fe_{0.19}Ni_{0.81}$ nanowire arrays shows a linear decreasing with increasing temperature, which can be understood by a phenomenological nucleate model.

PACS number(s): 75.50.Bb, 75.75.+a, 75.60.Jk

I. INTRODUCTION

The recent development of techniques allows the fabrication and the measurements of nanostructure magnetic materials, such as magnetic nanoparticles[1] and nanowire arrays.[2] Since the dimensions of these materials are reduced to values comparable to the domain-wall width, the interesting magnetic[1,3] and other physical properties[4] have been discovered. From the application point of view, artificial magnetic nanowires have a potential for ultrahigh density magnetic recording media.[2] Until now, much attention on magnetic nanowire arrays has been paid to the magnetic properties of metal[2,5] and alloy systems.[6,7]

Though pure magnetic metal nanowire arrays provide a model to investigate the magnetic properties of a quasi-one-dimensional system, a further limitation in magnetic parameters associated with these nanowire arrays will restrict the application to industry comparing the arrays of alloy nanowire, in which the magnetic parameters can be modified not only by the physical dimension but also by the composition.

Recently, Zhu *et al.*[8] reported the macromagnetic properties of the $Fe_{0.14}Ni_{0.86}$ nanowire array. Khan and Petrikowski[9] studied the magnetization and structural properties of soft magnetic $Fe_{26}Ni_{74}$ nanowires and the $Fe_{26}Ni_{74}$ layer. Ercole *et al.*[10] studied the finite size effects in the static and dynamic magnetic properties of the FeNi wire array. Then Adeyeye *et al.*[11] reported the magnetostatic interactions and magnetization reversal in $Fe_{80}Ni_{20}$ flat wire arrays using magnetoresistance measurements. Lee *et al.*[12] reported the effect of annealing temperature on the coercivity of the $Fe_{21}Ni_{79}$ nanowire array. Several aspects of the properties of the Fe-Ni nanowire array have been investigated in the above-mentioned works. However, the structure and magnetic properties for the large composition range of Fe-Ni have not been systematically investigated yet.

In the present work, we present the composition dependence of structure and magnetic properties in $Fe_{1-x}Ni_x$ nanowire array and the comparison with the bulk and particles system. The temperature dependence of magnetic properties of the $Fe_{1-x}Ni_x$ nanowire array is also presented.

II. EXPERIMENTAL

Arrays of $Fe_{1-x}Ni_x$ $(0 < x < 1)$ nanowire were produced by electrodepositing Fe^{2+} and Ni^{2+} into a porous alumina template (PAT). The details of preparation of PAT can be found elsewhere.[13] In this experiment, Al foils (99.999%) were annealed at 500 °C for about 48 h, then anodized at 40 V (dc) in 0.3 M $H_2C_2O_4$ aqueous solution at 15 °C for 1 h. After the porous templates were removed, the second anodized step was performed under the same conditions as above. Mixture aqueous solutions containing $FeSO_4 \cdot 7H_2O$, $NiSO_4 \cdot 6H_2O$, H_3BO_4, and ascorbic acid were used for electrodeposition, and the composition of the $Fe_{1-x}Ni_x$ nanowire can be adjusted by varying the $Fe^{2+}:Ni^{2+}$ ratio in the solution. The pH value of the electrolyte was maintained at about 3.0. Considering the difference of deposit rate between Fe^{2+} and Ni^{2+}, to ensure the same length of nanowire for a different Ni composition, all electrochemical depositions were conducted at 50 Hz, 13 V rms with deposition time ranging from 10 to 15 min. After deposition, samples were kept in pure alcohol solution to avoid oxidation. For convenience, the nanowire arrays with PAT were removed from the residual Al substrate by saturated aqueous solution of $HgCl_2$ before measuring x-ray diffraction (XRD) and magnetic properties. Nanowires were liberated from the PAT by dissolving it into an aqueous solution of NaOH before the observation with a transmission electron microscope (TEM).

Micromorphologies of the PAT and the nanowires were obtained by atomic force microscopy (AFM) (SPM-9500) and TEM (JEOL 2000), respectively. Detailed structural characterizations of nanowires were conducted by selected-areas electron diffraction (SAED) in the TEM observation. The crystal structure of nanowires with PAT was determined by XRD. The atomic percentages of the Fe and Ni in the nanowires were measured by an atomic absorption spectroscope (AAS). The magnetic properties of $Fe_{1-x}Ni_x$ nanowire arrays at various temperatures were measured using a vibrating-sample magnetometer (VSM) and a Quantum Design magnetometer [MPMS XL superconducting quantum interference device (SQUID)], respectively.

III. RESULTS AND DISCUSSION

A three-dimensional AFM image of the PAT prepared by the method mentioned above is shown in Fig. 1, displaying an ordered array of circular pores. The average diameter of
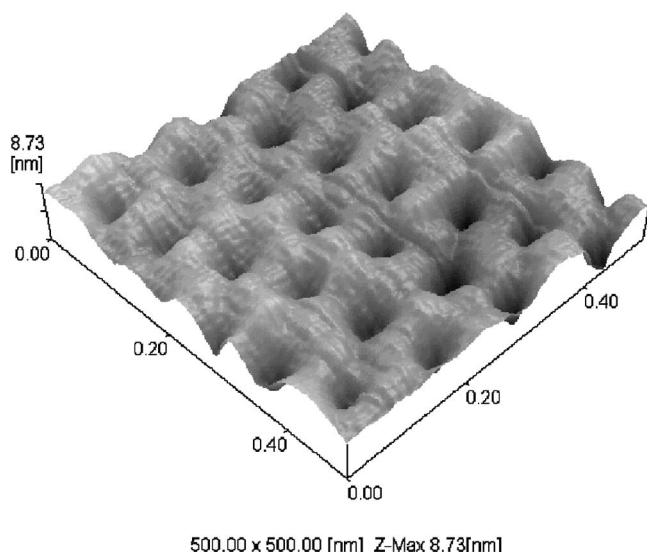
FIG. 1. AFM image of PAT with the pore diameter about 50 nm.

the pores is about 50 nm, and the bridge between adjacent pores is about 70 nm, which generates a pore density of about $5 \times 10^{10}/\text{cm}^2$. Similar results could also be found in Ref. 14, which a perfect pore structure is formed in alumina template except for a small difference of the pore parameter due to the different experimental condition.

Figure 2(a) shows a representative TEM image of $Fe_{1-x}Ni_x$ nanowires liberated from PAT, revealing that the nanowires have relatively regular cylindrical shape with about 50 nm in diameter. The length of nanowires is nearly uniform, and the longest nanowires are about 4 μm. Some shorter ones may be due to the breaking. For TEM observation, free nanowires were kept in a NaOH aqueous solution to avoid oxidation. The diameter of nanowires determined by TEM agrees well with the pore diameter in PAT. Nanowires are polycrystalline for all composition ranges as revealed by the dark field image as that in Ref. 15 and SAED. The representative SAED pattern of $Fe_{0.25}Ni_{0.75}$ nanowires shown in Fig. 2(b) demonstrates a face-centered cubic (fcc) structure. The diffraction rings correspond to the plane of (111), (200), (220), and (311), respectively.

Dependence of Ni content in $Fe_{1-x}Ni_x$ nanowires (obtained by AAS) on the ratio of $Ni^{2+}:Fe^{2+}$, a, in the electrolyte is shown in Fig. 3. It appears that the Ni content x increases with increasing ratio a. It is known that Ni is less electronegative than that of Fe according to the theory of galvano-electrochemistry. Therefore, the deposit rate of Ni should be higher than that of Fe. However, the Ni content, x, is about 0.5 when $a=7$, indicating the deposit rate of Ni^{2+} is lower than that of Fe^{2+}. The anomalous codeposition phenomenon has also observed in depositing the Fe-Ni film.[16] Furthermore, in Fig. 3, there are two different slopes in the x versus a curve. The slope for $a<10$ is much larger than that for $a>10$, despite the x linear increasing with a in both two ranges. This phenomenon can be ascribed to the changes of kinetic mechanism as Ni^{2+} ions increase and confirmed by measuring the current density of electrodeposition.

Figure 4 presents the XRD patterns of $Fe_{1-x}Ni_x$ nanowire arrays, the circular and triangle dots denote the body-
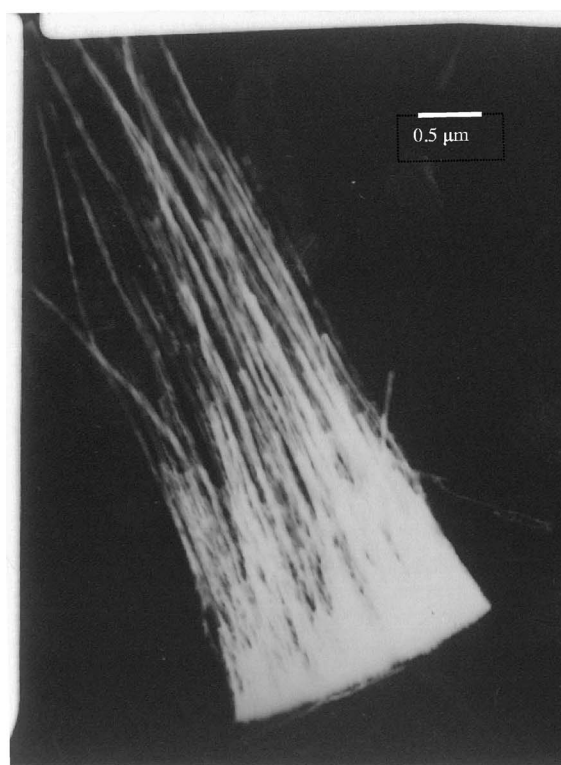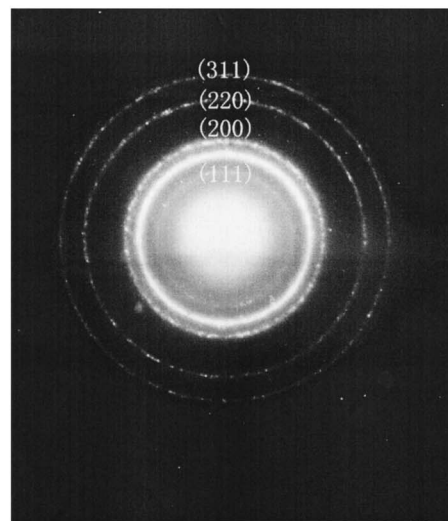
FIG. 2. (a) TEM image of the nanowires with about 50 nm in diameter, longest wires are about 4 μm. (b) The SAED patterns of the $Fe_{0.25}Ni_{0.75}$ nanowires.

centered cubic (bcc) and fcc phases, respectively. Since all PATs have an amorphous structure, there are no diffraction peaks corresponding to them. The results show that the $Fe_{1-x}Ni_x$ nanowire arrays have a bcc structure alone for $x<0.35$, a mixed phase of bcc and fcc coexists for $0.35<x<0.5$ and only a fcc phase for $x>0.5$. The phase transition, from bcc to fcc, of $Fe_{1-x}Ni_x$ nanowire arrays is similar to those of bulk[17] and particles[18] of the Fe-Ni alloy. However, the mixture phase in the bulk and particle systems occurred in the range of $0.05<x<0.72$,[17] and $0.2<x<0.4$,[18] respectively. The region of the x value corre-
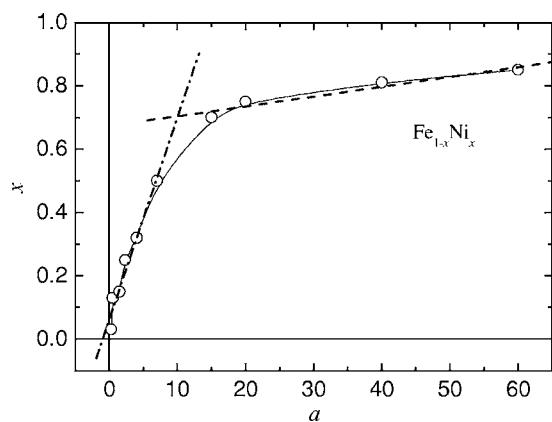
FIG. 3. Variations of Ni content x in the nanowires as a function of $Ni^{2+}:Fe^{2+}$ ratio a in the solution. The solid line is a guide to the eyes. The dotted-dashed and dashed lines are the linear fitting results for $a < 10$ and $a > 10$, respectively.

sponding to the two-mixed-phase coexistence is narrower for nanowires than that for bulk and particles. Comparing to Fe-Ni particles fabricated by the method of hydrogen plasma reaction,[18] this region goes to a high Ni content in $Fe_{1-x}Ni_x$ nanowire array system. The similar phenomenon is also observed in other nanowire systems.[19] The difference of phase boundary between nanowires and particles can probably be attributed to the electrochemical deposition method in which there is one dimension free (long axis) to grow and two dimensions (diameter) limited. On the other hand, the deposit rate of Fe^{2+} is much higher than that of Ni^{2+}, which indicates that the bcc structure (like Fe) forms more easily than the fcc structure (like Ni) and results in the bcc-fcc mixed composition range shifting to a high Ni composition.

In order to investigate the magnetic properties of $Fe_{1-x}Ni_x$ nanowire arrays, hysteresis loops and initial magnetization curves for all samples have been measured at various temperatures. The hysteresis loops were measured with the ap-
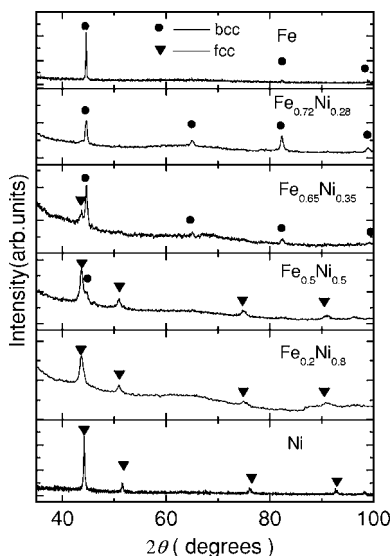

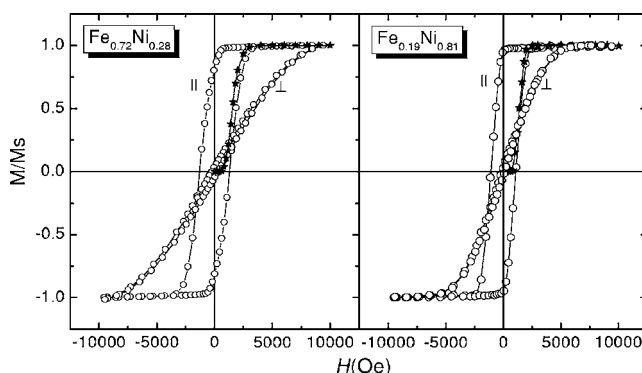FIG. 4. XRD patterns of PAT filled with $Fe_{1-x}Ni_x$ nanowire arrays.

FIG. 5. The hysteresis loops and initial magnetization curves of the $Fe_{0.72}Ni_{0.28}$ and $Fe_{0.19}Ni_{0.81}$ nanowire arrays with the applied field parallel (∥) and perpendicular (⊥) to the long axis of nanowires. The asterisk denotes the initial magnetization curves.

plied field parallel (∥) and perpendicular (⊥) to the long axis of nanowires, while the initial magnetization curves were measured with the applied field parallel to the long axis direction (∥). Figure 5 shows typical results for two nanowire arrays of $Fe_{0.72}Ni_{0.28}$ and $Fe_{0.19}Ni_{0.81}$ at 300 K, which exhibit bcc and fcc structure, respectively. The shape of hysteresis loops of other samples with different Ni content and temperature are similar to Fig. 5, but the magnetic parameters, such as coercivity, saturated magnetization, and remanence, are different. Comparing the hysteresis loops between the field parallel and perpendicular to the long axis for these two samples, it was found that the easy axis of nanowires is parallel to its long axis in spite of their different structure. Similar results have been also reported in the other magnetic nanowire arrays systems.[20] This is because of the strong shape anisotropy. Mössbauer-effect results, in which the static magnetic moments are all parallel to the long axis of nanowires,[15,21] support this point. It was also found that the magnetic moment cannot reverse until the applied field gets to a critical value, suggesting a high-energy barrier between the two states. In addition, it is apparent that the saturated field of $Fe_{0.19}Ni_{0.81}$ nanowire arrays in a perpendicular direction is smaller than that of the $Fe_{0.72}Ni_{0.28}$ nanowires.

Figure 6(a) shows the coercivity (H_c) versus Ni content and Fig. 6(b) shows the squareness (M_r/M_s) of the hysteresis loops versus Ni content for $Fe_{1-x}Ni_x$ nanowire arrays at 300 K. With increasing x, the coercivity with the applied field parallel to the long axis decreases linearly first and reaches minimum at $x = 0.5$, and then increases to a maximum near $x = 0.7$, then decreases again when $x > 0.7$. This interesting tendency may be attributed to the changes of the saturated magnetization, which is controlled by the structure and content of the samples. Due to the complicated tendency with Ni composition in Fe-Ni bulk alloy and the difficulty of measuring the accurate mass of nanowires in PATs, the saturated magnetization in nanowire arrays is in progress and the results will be discussed later. In Fig. 6(b), the squareness (M_r/M_s) with the applied field parallel to the long axis is greater than 0.8 and obviously larger than that with the applied field perpendicular to the long axis for all $Fe_{1-x}Ni_x$ ($0 < x < 1$), indicating again that the samples have a strong magnetic anisotropy with easy direction parallel to the
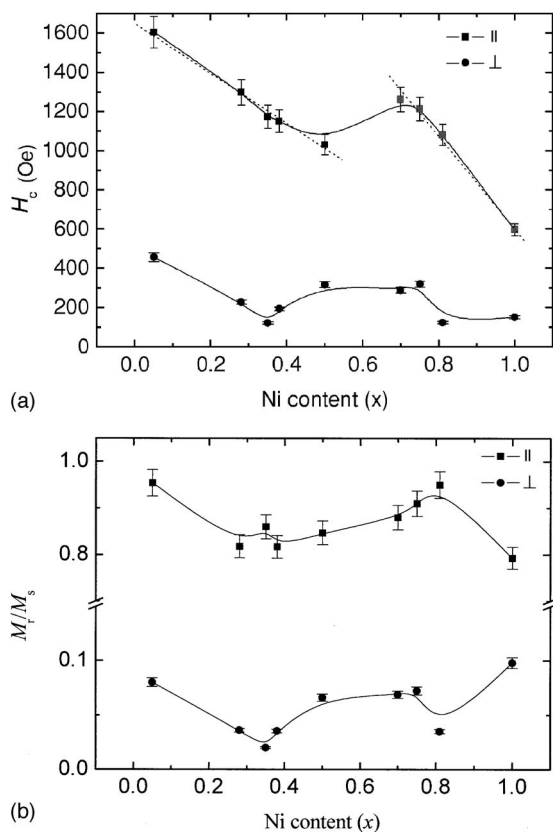
(a)

(b)

FIG. 6. (a) The coercivity (H_c) versus Ni content (x) for the Fe$_{1-x}$Ni$_x$ nanowire array at 300 K. Solid lines are guides to the eyes. The dashed lines are the linear fitting results for $x < 0.5$ and $x > 0.5$, respectively. (b) The squareness (M_r/M_s) versus Ni content for the Fe$_{1-x}$Ni$_x$ nanowire array at 300 K. Solid lines are guides to the eyes.

long axis and perpendicular to the surface of PAT. Comparing with Fe-Ni bulk alloys, which have isotropic soft magnetic property with small coercivity for about several Oe, nanowire systems exhibit larger coercivity and squareness.

Figures 7(a) and 7(b) show the temperature (T) dependence of H_c for two typical samples, Fe$_{0.68}$Ni$_{0.32}$ and Fe$_{0.19}$Ni$_{0.81}$, with the applied field parallel to the long axis of nanowires. It is apparent that the H_c was nearly linear over a temperature range of 5–300 K. This tendency is in contrast with the models of nucleation due to the thermal activation, in which there is a relationship of H_c with $T^{1/2}$. Therefore, how to understand the linear relationship of H_c with T is a fundamental problem.

It is well known that the influence of temperature on the magnetization reversal is usually proceeded by changing the intrinsic magnetic parameters, such as the saturated magnetization (M_s), the magnetocrystalline anisotropy constant, etc. Considering the accurate mass of nanowires could not be obtained, the temperature dependence of magnetization (M) with a saturated field is given in Fig. 8. M decreases with increasing temperature and obeys the $T^{3/2}$ law. Since the nanowire mass does not depend on the temperature, the T dependence of M will show the correct temperature dependence of M_s, which indicating M_s can be expressed as[22]
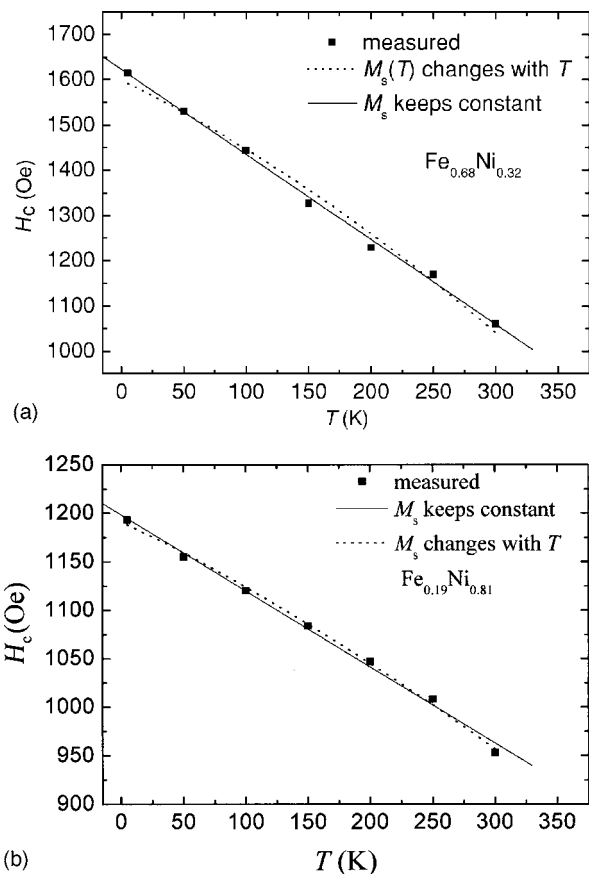

(a)

(b)

FIG. 7. Temperature dependence of coercivity, H_c, (a) for Fe$_{0.68}$Ni$_{0.32}$ and (b) for Fe$_{0.19}$Ni$_{0.81}$ nanowire arrays. Solid squares in (a) and (b) denote the measured data. Solid lines in (a) and (b) are linear fitting results of Eq. (4) with temperature being independent of M_s. The dotted lines in (a) and (b) are the fitting results of Eq. (5) with $M_s(T)$ changing with temperature at $T^{3/2}$.

$$M_s(T) = M_s(0)(1 - CT^{3/2}). \tag{1}$$

Here $M_s(T)$ and $M_s(0)$ are the values at a temperature of T and 0 K, respectively. The magnetocrystalline anisotropy
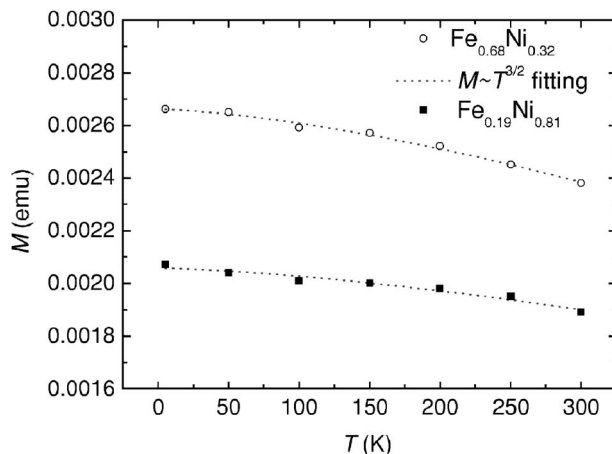

FIG. 8. The temperature (T) dependence of M with a saturated field parallel to the long axis of the nanowire.

constant (K_1) decreases with increasing Ni content, from 4.2×10^4 J/m^3 with $x=0$ (Fe) to -4.8×10^3 J/m^3 with $x=1$ (Ni),[23,24] and can be omitted when comparing to the shape anisotropy.[13] The XRD and electron diffraction results show that the nanowire arrays are polycrystalline, therefore, no major contribution from the magnetocrystalline anisotropy would be expected. Figures 7(a) and 7(b) show that, with the temperature increasing from 5 K to 300 K, the coercivity decreases about 50% and 30% for Fe$_{0.68}$Ni$_{0.32}$ and Fe$_{0.19}$Ni$_{0.81}$ nanowire arrays, respectively. While the saturated magnetization decreases only about 10%. This indicates that there is another more important factor to influence the temperature dependence of coercivity.

Considering the large shape anisotropy and demagnetization energy, the magnetic moments for the domains in the nanowires should be parallel or antiparallel to the long axis. Assume that two stable magnetic states, that is, moments "up" and "down," correspond to the parallel and antiparallel states, the nanowire system could be considered as a bistable system.[25] The two states are separated by an energy barrier. As the temperature increases, some magnetic moments will overcome the energy barrier and the magnetization reverses. The result is similar to that of an equivalent applied field to reverse the magnetization. The thermal fluctuations will influence the magnetization reversal.

Temperature dependence of coercivity can be understood based on the above bistable-state thermal fluctuation model. Assume that the magnetization reversal started from a reversal magnetization nucleus with the activation volume v. The energy barrier involved in the magnetization reversal is expressed by[26]

$$E = E_0 + H \frac{\partial E}{\partial H}, \qquad (2)$$

where E_0 is the field independent part of E. $\partial E / \partial H$ is related to the magnetic viscosity coefficient. At the coercive field, it may be written, taking into account thermal activation effects,[27] that

$$E_0 + H_c \frac{\partial E}{\partial H} = 25 k_R T, \qquad (3)$$

where k_B and T is the Boltzmann constant and temperature, respectively. During the magnetization reversal process, two energy terms are expected to contribute to the energy barrier E_0, that is, the domain-wall energy and the magnetostatic energy. Since nucleation of a single π-domain wall at the end of wire leads to smaller energy barrier,[28] the domain-wall energy can be derived by $E_p = \gamma s$, where γ represent the energy density of the domain wall and s is the surface of the activation volume. The magnetostatic energy $E_d = \alpha 4 \pi M_s^2 v$, where M_s is the saturation magnetization and α is a phenomenological parameter. Thus,

$$H_c = \alpha 4 \pi M_s - \frac{\gamma s}{v M_s} - \frac{25 k_B T}{v M_s}. \qquad (4)$$

The activation volume v is proportional to $\sqrt{A/K_{eff}}$ and $\gamma = 4\sqrt{A K_{eff}}$,[29] where A is the exchange stiffness constant. In molecular field theory, the exchange stiffness constant varies as S^2, where S is the spin, and hence A is expected to vary with M_s^2. K_{eff} is the effective anisotropy constant. In our nanowires system, the contribution from magnetocrystalline anisotropy can be omitted due to the polycrystalline structure and the shape anisotropy has the main contribution on K_{eff}. We assume that it is similar to a uniaxial anisotropy and K_{eff} is thus proportional to M_s^2.[25]

If we assume that M_s is a constant at low temperature due to the high Curie temperature, thus γ and v are independent of the temperature, which means that coercivity is linearly dependent on the temperature. The fitting results for the Fe$_{0.68}$Ni$_{0.32}$ and Fe$_{0.19}$Ni$_{0.81}$ nanowires are shown in Figs. 7(a) and 7(b), respectively, with the saturation magnetization M_s derived from the bulk Fe-Ni alloy.[30,31] It can be found that the experimental results of coercivity agree well with the linear temperature dependence predicted by Eq. (4). This result is consistent with the Fe nanowire-filled carbon nanotube.[32] The fitting activation volumes for two samples are about 1×10^3 nm^3 and 9×10^3 nm^3, respectively. The value of α, 0.07 and 0.2, for these two samples may indicate that the nucleation starts from the end of the nanowires; the experimental proof has been found by Mössbauer spectra results,[21] and other calculations gave the similar behavior.[33] The T dependence of H_c of the other Fe-Ni alloy nanowire array shows a similar tendency, although the parameters are different.

Since M_s changes about 10% in the temperature range 5–300 K, we now consider the influence of M_s to Eq. (4). The second term $\gamma s / v M_s \propto 4 s \sqrt{A K_{eff}} / \sqrt{A / K_{eff}} M_s = k M_s$, thus Eq. (4) becomes

$$H_c = K M_s(T) - \frac{25 k_B T}{v M_s(T)}, \qquad (5)$$

where K is another phenomenological parameter. $M_s(T)$ is determined by Eq. (1). The fitting result by Eq. (5) is also shown in Fig. 7, in which the $M_s(0)$ derived from the bulk materials and the parameter C in Eq. (1) is derived by fitting the experimental data in Fig. 8. It can be found that the fitting result is still perfect with the experimental data. The coercivity is nearly linear with temperature, in spite of the $T^{3/2}$ law of saturated magnetization. This result indicates that the temperature dependence of M_s has a minor effect on coercivity, and about 10% of the changes to M_s will not obviously change the linear temperature dependence of coercivity. The fitting activation volume (1.4×10^3 nm^3 and 1.3×10^4 nm^3 for Fe$_{0.68}$Ni$_{0.32}$ and Fe$_{0.19}$Ni$_{0.81}$, respectively) are larger than the case where M_s is independent of temperature. The reason for this result is that the decreasing of M_s will help more magnetic moments reverse and thus lead to a larger activation volume. It is worth noting that the model predicted by Eq. (4) is different from the actual nucleation mode. It is only a phenomenological model to interpret the results of hard magnetic materials.[27]

IV. CONCLUSION

In summary, the fabrication, structure, and magnetic properties of the Fe$_{1-x}$Ni$_x$ nanowire array have been studied sys-

tematically and compared with bulk or particles. AFM and TEM results show that the diameter of nanowires is about 50 nm, and the length is about 4 μm. Structure study by SAED and XRD shows that the $Fe_{1-x}Ni_x$ nanowire arrays have a bcc structure alone for $x < 0.35$, a mixed phase of bcc and fcc coexists for $0.35 < x < 0.5$, and only a fcc phase for $x > 0.5$. The phase boundary of $Fe_{1-x}Ni_x$ nanowires array is different from that of the bulk and particle system. The hysteresis loops at various temperatures are studied. The dependence of coercivity on Ni content (x) at 300 K, with the applied field parallel to the nanowires, shows that the coercivity linearly decreases with both $x < 0.5$ and $x > 0.7$, while in the range of 0.5 to 0.7, the coercivity increase with in-creasing of x. The coercivity with the applied field along the long axis linearly decreases with increasing temperature is found for the $Fe_{0.68}Ni_{0.32}$ and $Fe_{0.19}Ni_{0.81}$ nanowire arrays, which are interpreted by a phenomenological nucleate model.

*Author to whom correspondence should be addressed. Email address: liuqf@lzu.edu.cn or liuqingfang@gmail.com

[1] L. Del Bianco, C. Ballesteros, J. M. Rojo, and A. Hernando, Phys. Rev. Lett. **81**, 4500 (1998).

[2] T. M. Whitney, J. S. Jiang, P. Searson, and C. Chien, Science **261**, 1316 (1993).

[3] S. Dubois, J. Colin, J. L. Duvail, and L. Piraux, Phys. Rev. B **61**, 14315 (2000).

[4] C. Beeli, Nanostruct. Mater. **11**, 697 (1999).

[5] J. I. Martin, J. Nogues, I. K. Schuller, M. J. Van, K. Temst, C. V. Haesendonck, V. V. Moshchalkov, and Y. Bruynseraede, Appl. Phys. Lett. **72**, 255 (1998).

[6] A. Ercole, A. O. Adeyeye, C. Daboo, J. A. C. Bland, and D. G. Hasko, J. Appl. Phys. **81**, 5452 (1997).

[7] H. J. Blythe, V. M. Fedosyuk, O. I. Kasyutich, and W. Schwarzacher, J. Magn. Magn. Mater. **208**, 251 (2000).

[8] H. Zhu, S. G. Yang, G. Ni, S. L. Tang, and Y. W. Du, J. Phys.: Condens. Matter **13**, 1727 (2001).

[9] H. R. Khan and K. Petrikowski, J. Magn. Magn. Mater. **213**, 526 (2000).

[10] A. Ercole, A. O. Adeyeye, C. Daboo, J. A. C. Bland, and D. G. Hasko, J. Appl. Phys. **81**, 5452 (1997).

[11] A. O. Adeyeye, J. A. C. Bland, C. Daboo, and D. G. Hasko, Phys. Rev. B **56**, 3265 (1997).

[12] K. H. Lee, H. Y. Lee, W. Y. Jeung, and W. Y. Lee, J. Appl. Phys. **91**, 8513 (2002).

[13] Q. F. Liu, C. X. Gao, J. J. Xiao, and D. S. Xue, J. Magn. Magn. Mater. **260**, 151 (2003).

[14] A. P. Li, F. Muller, A. Birmer, K. Nielsch, and U. Gosele, J. Appl. Phys. **84**, 6023 (1998).

[15] J. B. Wang, Q. F. Liu, D. S. Xue, Y. Peng, X. Z. Chao, and F. S. Li, J. Phys. D **34**, 1 (2001).

[16] J. Harkans, J. Electrochem. Soc. **128**, 45 (1981).

[17] T. B. Massalsky, *Binary Alloy Phase Diagrams*, 2nd ed. (ASM International, Ohio, 1990).

[18] X. G. Li, A. Chiba, and S. Takahashi, J. Magn. Magn. Mater. **170**, 339 (1997).

[19] Q. F. Zhan, Z. Y. Chen, D. S. Xue, F. S. Li, H. Kunkel, X. Z. Zhou, R. Roshko, and G. Williams, Phys. Rev. B **66**, 134436 (2002).

[20] R. Ferre, K. Ounadjela, J. M. George, L. Piraux, and S. Dubois, Phys. Rev. B **56**, 14066 (1997).

[21] J. B. Wang, X. Z. Zhou, Q. F. Liu, D. S. Xue, F. S. Li, B. Li, H. P. Kunkel, and G. Willimas, Nanotechnology **15**, 485 (2004).

[22] C. Herring and C. Kittel, Phys. Rev. **81**, 869 (1951).

[23] L. P. Tarasov, Phys. Rev. **56**, 1245 (1939).

[24] R. M. Bozorth and J. G. Walker, Phys. Rev. **89**, 624 (1953).

[25] B. Giorgio, *Hysteresis in Magnetism (For Physics, Materials Scientists, and Engineers)* (Academic Press, Inc., New York, 1998).

[26] D. Givord, A. Lienard, P. Tenaud, and T. Viadieu, J. Magn. Magn. Mater. **67**, L281 (1987).

[27] D. Givord, P. Tenaud, and T. Viadieu, IEEE Trans. Magn. **24**, 1921 (1988).

[28] J. E. Knowles, J. Magn. Magn. Mater. **61**, 121 (1986).

[29] H. B. Braun, Phys. Rev. B **50**, 16501 (1994).

[30] E. I. Kondorsky and V. L. Sedov, J. Appl. Phys. **31**, 331S (1960).

[31] R. M. Bozorth, *Ferromagnetism* (D. Van Nostrand, New York, 1951).

[32] N. Grobert, W. K. Hsu, Y. Q. Zhu, J. P. Hare, H. W. Kroto, and D. R. M. Walton, Appl. Phys. Lett. **75**, 3363 (1999).

[33] E. D. Boerner and H. N. Bertram, IEEE Trans. Magn. **33**, 3052 (1997).